PHILOSOPHICAL TRANSACTIONS OF THE ROYAL SOCIETY A MATHEMATICAL, PHYSICAL & ENGINEERING SCIENCES

Time-Resolved Diffraction Studies on Glycogen Phosphorylase b

E. M. H. Duke, A. Hadfield, S. Walters, S. Wakatsuki, R. K. Bryan and L. N. Johnson

Phil. Trans. R. Soc. Lond. A 1992 **340**, 245-261
doi: 10.1098/rsta.1992.0064

Time-resolved diffraction studies on glycogen phosphorylase *b*

By E. M. H. Duke, A. Hadfield, S. Walters, S. Wakatsuki, R. K. Bryan and L. N. Johnson

Laboratory of Molecular Biophysics, University of Oxford, Rex Richards Building, South Parks Road, Oxford OX1 3QU, U.K.

Glycogen phosphorylase catalyses the reversible phosphorylation of glycogen to give glucose-1-phosphate in a reaction mechanism promoted by the 5′-phosphate of the cofactor pyridoxal phosphate. The reaction with the small substrate heptenitol has been probed using Laue diffraction at the Synchrotron Radiation Source, Daresbury. The reaction was initiated following photolysis from a caged phosphate compound 3,5-dinitrophenylphosphate (DNPP). In measurements on photolysis in the crystal using a diode array spectrophotometer approximately 7 mM cage (and hence phosphate) was released from a 21 mM solution with five flashes from a xenon flash lamp. In an experiment with the home source it was shown that DNPP is stable in the crystal under conditions of X-ray measurements and that on flashing sufficient phosphate is released to promote catalysis within 24 h. In a similar experiment with the synchrotron and Laue diffraction, data were recorded before and then 3 min, 15 min and 1 h after initiation of the reaction. Theoretical analysis of the point spread function arising from partial data-sets, numerical calculations with ideal data and the experimental results have shown the importance of low-resolution terms for the interpretation of Laue difference maps. Inclusion of terms obtained from unscrambling the wavelength harmonic overlaps led to significant improvement. The maps showed heptenitol bound at the catalytic site but no evidence for catalysis under these conditions. A rational for the lack of reaction and suggestions for future experiments with improved data are outlined.

1. Introduction

Glycogen phosphorylase (EC. 2.4.1.1) catalyses the intracellular phosphorolysis of glycogen to yield glucose-1-phosphate (Glc-1-P)

$$(\alpha\text{-1,4-glucoside})_n + P_i \leftrightarrow (\alpha\text{-1,4-glucoside})_{n-1} + \text{Glc-1-P}.$$

The enzyme contains stoichiometric amounts of pyridoxal 5′-phosphate (PLP) linked via a Schiff base to Lys 680 and the 5′-phosphate group of the cofactor plays an obligatory role in catalysis. This paper describes progress in time-resolved studies aimed at answering a specific biochemical question. How does the enzyme promote attack of phosphate on the C1 carbon of the glycosidic bond and allow the reaction to proceed in the direction of phosphorolysis and not hydrolysis?

Phosphorylase is an archetypal control enzyme. It exhibits regulation both by reversible phosphorylation and by allosteric effectors and integrates diverse signals

Phil. Trans. R. Soc. Lond. A (1992) **340**, 245–261
Printed in Great Britain

associated with ligand binding at five spatially distinct sites. To a first approximation these effects can be understood in terms of an equilibrium between several conformational states ranging from a low affinity T state to a high affinity R state according to the model of Monod, Wyman and Changeux. The major effect of the allosteric transition is to increase the affinity for phosphate or Glc-1-P (Helmreich & Cori 1964). The K_D for phosphate has been estimated to be 93 mM for the free enzyme, 15 mM for the enzyme–AMP complex and 2.2 mM for the enzyme–AMP–glycogen complex (reviewed in Johnson *et al.* 1989).

The catalytic site is situated at the centre of the subunit removed from the subunit–subunit interface of the functional dimer but connected to it by the 280s loop of chain. The site is buried some 15 Å† from the bulk solvent at the base of a narrow tunnel formed by the interface of the two domains of the subunit and close to the essential cofactor PLP (see Acharya *et al.* (1991) or Barford & Johnson (1989) for figures of the whole molecule). In the T state access to the catalytic site is restricted by a loop of chain termed the 280s loop (residues 282 to 285) and Asp 283 points into the catalytic site linked via two water molecules to the 5′-phosphate of PLP (Oikonomakos *et al.* 1987; Acharya *et al.* 1991). On conversion to the R state the 280s loop is displaced, His 571 breaks its hydrogen bond with Asp 283 and forms a new interaction with Tyr 613, Arg 569 replaces the acidic group Asp 283 and access to the catalytic site is available (Barford & Johnson 1989). The mutual interchange between the acidic group and the basic group appears to be the major change on the T to R conversion that provides a high affinity phosphate recognition site in the R state (Barford & Johnson 1989; Barford *et al.* 1991).

Early kinetic studies had shown that the enzyme is active in the crystalline state and exhibits about a 30 fold decrease in rate compared with the enzyme in solution and similar K_m values for substrates oligosaccharide and Glc-1-P (Kasvinsky & Madsen 1976). X-ray experiments on catalysis in the crystal (Hajdu *et al.* 1987*a*) showed that the reaction could be followed either in the direction of oligosaccharide breakdown or synthesis. Because of the difficulties in locating oligosaccharide at the catalytic site, the most informative studies on the catalytic mechanism in the T state have used the small substrate heptenitol. In the presence of phosphate, phosphorylase catalyses the non-reversible phosphorylation of heptenitol to the product heptulose-2-phosphate (β-1-C-methyl,α-D-glucose-1-phosphate) (Klein *et al.* 1986) (see figure 1). Heptulose-2-P is a potent inhibitor with a $K_i = 14\ \mu$M in solution. The product is bound with considerably higher affinity than the closely related substrate (or product) Glc-1-P, where K_D is about 3 mM and heptulose-2-P has characteristics of a transition state analogue. The crystal structure of the T state GP*b*-heptulose-2-P complex has been refined at 2.9 Å resolution (Johnson *et al.* 1990). The product is firmly bound at the catalytic site and exhibits temperature factors that are comparable with the most well ordered regions of the enzyme. The major conformational change involves the movement of an arginine residue (Arg 569) from a position buried in the protein to a new position in which the guanidinium group contacts the product phosphate. The shift is similar to that observed on conversion to the R state. However, lattice forces prevent the T to R state allosteric transition and instead of the displacement of the 280s loop, Asp 283 and Asn 284 undergo localized changes so that Asp 283 occupies a site close to that previously occupied by Arg 569.

† 1 Å = 10^{-10} m = 10^{-1} nm.

PHILOSOPHICAL TRANSACTIONS OF THE ROYAL SOCIETY A MATHEMATICAL, PHYSICAL & ENGINEERING SCIENCES

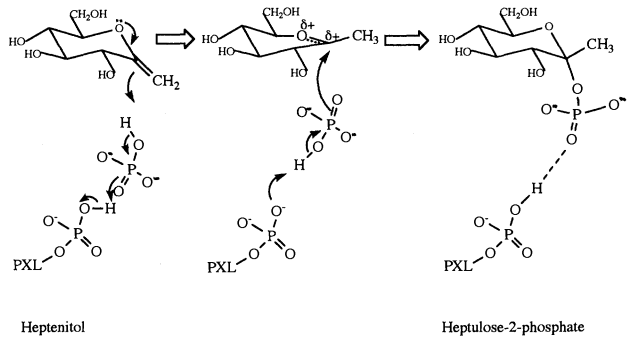

Figure 1. A schematic diagram of the proposed mechanism for the enzyme catalysed phosphorolysis of heptenitol to heptulose-2-phosphate. For further details see text.

The evidence leading to the proposals for the catalytic mechanism and the role of the cofactor 5′ phosphate group have been reviewed (Madsen & Withers 1986; Johnson *et al.* 1989; Palm *et al.* 1990). The proposals put forward on the basis of the crystallographic results (Johnson *et al.* 1990) with T state GP*b* and now supported by studies with R state GP*b* and R state GP*a* complement those deduced from the results of kinetics and NMR experiments and demonstrate the additional contribution of stereoelectronic effects. The structures observed favour a mechanism (figure 1) in which phosphorylysis of heptenitol is catalysed by general acid attack of the substrate phosphate promoted by the cofactor phosphate. The proton is donated by the substrate phosphate in a concerted reaction in which it immediately gains a proton from the cofactor phosphate. After protonation of the methylene carbon, the glucosyl carbonium ion is stabilized by the negatively charged substrate phosphate group. No covalent intermediate has been detected in phosphorylase catalysis and the structure of the protein provides no suitable candidates for a covalent glucosyl intermediate, hence it is assumed that the reaction proceeds through a carbonium ion intermediate. The reaction is completed by nucleophilic attack of the substrate phosphate on the carbonium ion to give the product heptulose-2-P. The transition state stabilization by the substrate dianion within the confined and shielded environment of the catalytic site means that the reaction can proceed only in the direction of phosphorolysis and not hydrolysis. The mechanism can be readily extended to the natural reaction.

In a series of time-resolved experiments that exploited the brilliance of the synchrotron radiation source at Daresbury the conversion of heptenitol to heptulose-2-P was followed in the crystal in which the earliest time shot was recorded about 1 h after initiation of the reaction with conventional oscillation monochromatic wavelength methods (Hajdu *et al.* 1987*a*). This gave a tantalizing glimpse of what might be phosphate in the attacking position. In this paper we describe progress in experiments designed to follow the phosphorylase reaction in the crystal on a finer timescale using Laue diffraction. The rate limiting step in the phosphorylase reaction is the turnover the ternary enzyme–substrate complex (Engers & Madsen 1970) and the hope is that, providing measurements are fast enough, this complex might be observed and the turnover to product subsequently followed in the same crystal. There is a special interest in identifying the phosphate position in the attacking stage and following the involvement of Arg 569 in the catalytic process. The roles of other ionic groups in the vicinity are also of interest. Site directed mutagenesis studies with

E. coli maltodextrin phosphorylase (Schninzel & Palm 1990; Schninzel & Druekes 1991) have shown that there is a decrease in rate of about 500 fold when Glu 672 is changed to aspartic acid or glutamine and there is an increase in the error rate of hydrolysis over phosphorolysis. (In *E. coli* wild-type maltodextrin phosphorylase the error rate is less than 1 in 9000.) The crystal structure of the product complex shows that the role of Glu 672 is two fold: it serves to bind the 2 and 3 OH groups of the glucosyl substrate and to localize other polar and ionic groups (Tyr 573 and Lys 574) in the vicinity. Do these and other ionic groups have a more dynamic function than localization through binding and maintenance of correct electrostatic environment, and exclusion of attack by water?

2. Caged phosphate in X-ray experiments

In previous work initiation of the reaction had been achieved by diffusion of substrate into the crystal. Diffusion is rapid ($t_{\frac{1}{2}} < 1$ min for inorganic phosphate and about 1.8 min for Glc-1-P (Johnson & Hajdu 1989)) but a transient disorder is observed in the crystals on diffusion of phosphate compounds that takes about 7 min to heal. Thus there is a dead time of about 8–10 min before X-ray measurements can start and during this time some enzyme molecules are likely to turnover substrate. Therefore for Laue experiments the use of caged phosphates has been explored to provide closer synchrony of the start of the reaction with the start of X-ray measurements. A caged compound is a photosensitive precursor molecule that has been made biologically inert through covalent attachment of a photosensitive group (Kaplan *et al.* 1978; McCray & Trentham 1989). The caged substrate can be diffused into the crystal and then activated at the required time by photolysis to yield substrate. The most widely used caged phosphates are derivatives 1-(2-nitrophenyl)ethyl phosphate but the liberated cage rearranges to a nitrosoketone that is reactive with thiols and other nucleophiles on the protein. In many studies such unwanted reaction can be blocked by the inclusion of a reducing agent such as dithiothreitol (DTT). For phosphorylase high concentrations of phosphate are required for the enzyme in the T state and the crystals crack in the presence of DTT. Hence the development by Trentham and his colleagues (Corrie *et al.* 1992) of a new caged phosphate 3,5-dinitrophenyl phosphate (DNPP) has been of particular interest to us. DNPP is photosensitive and is converted to 3,5-dinitrophenol and P_i by irradiation at 300–360 nm with reasonable quantum efficiency. The absorption spectrum of DNPP is similar but not identical to dinitrophenol (protonated form). The extinction coefficients of 3,5-dinitrophenol at wavelengths of absorption maxima, 252 and 340 nm are 15300 and 3100 M^{-1} cm^{-1} respectively. The photolysis of DNPP can be measured by release of 3,5-dinitrophenolate ($pK_a = 6.8$) with extinction coefficient at wavelengths of absorption maxima, 268 and 400 nm, 13000 and 2800 M^{-1} cm^{-1} respectively (Parke 1961).

Photolysis of DNPP has been monitored in the crystal with an Oriel diode array spectrophotometer specially adapted with fibre optic light paths for crystal measurements (A. Hadfield and J. Hajdu, unpublished work). The instrument can record spectra within a time resolution of 20 ms for wavelength range 200–800 nm. Crystals of rabbit muscle GP*b* T state, space group $P4_32_12$, unit cell parameters $a = b = 128.5$ Å, $c = 116.3$ Å were transferred to thin walled quartz capillary tubes and soaked in solutions containing DNPP in 10 mM Bes buffer, 10 mM magnesium acetate

PHILOSOPHICAL TRANSACTIONS OF THE ROYAL SOCIETY A MATHEMATICAL, PHYSICAL & ENGINEERING SCIENCES

at pH 6.7 for 10 min. DNPP was a generous gift from Dr D. R. Trentham and G. P. Reid (National Institute for Medical Research, Mill Hill). The release of cage was effected by a series of 1 ms flashes (approximately 100 mJ per flash) from a high intensity xenon flashlamp (Hi-Tech Scientific, Salisbury, U.K. (Rapp & Guth 1988)) into a spot approximately 2 mm in diameter focused on the crystal at a distance of about 20 mm from the lamp. The wavelength range for illumination of the crystal was restricted to 300–400 nm with a UG11 filter. The lamp requires a recovery period of 5 s between flashes.

A crystal (dimensions 0.32 mm × 0.2 mm × 2 mm) was soaked in a solution containing 21 mM DNPP in 10 mM Bes buffer, 10 mM magnesium acetate, pH 6.7 and mounted as described above. Forty spectra were recorded every 20 s and between each spectrum the crystal was flashed. Under these conditions the whole surface area of the crystal facing the lamp (0.2 mm × 2.0 mm) was irradiated and the pathlength for transmission was 0.32 mm. The increase in absorbance at 400 nm was used to measure the concentration of the released 3,5-dinitrophenolate and the concentration corrected for the nitrophenol/nitrophenolate equilibrium (pK 6.8) at pH 6.7 to give the total phosphate released. It was found that approximately 5–6% of the total concentration of DNPP available was released per flash. After five flashes the concentration of phosphate was about 7 mM (32% liberation). After 10 flashes, the concentration was 10 mM (50%) and after 25 flashes 17 mM (82%). Additional work has shown that more product is released per flash if the crystal is rotated between flashes consistent with the notion that the absorbance of the caged compound may prevent light reaching the far side of the crystal to initiate release of the cage. These experiments need to be extended to cover release under different concentrations and different thicknesses of crystals to establish more quantitative values. Nevertheless the preliminary measurements suggest reasonably efficient release under the conditions used in the X-ray experiments.

To test if the amount of phosphate released was sufficient to promote catalysis an experiment was carried out with the home X-ray facilities (Duke *et al.* 1991). Two crystals were soaked in solutions containing 50 mM heptenitol, 30 mM DNPP, 10 mM Bes, 10 mM magnesium acetate at pH 6.7. Heptenitol was synthesized by Dr G. W. R. Fleet and I. Bruce (Dyson Perrins Laboratory, Oxford) following the method of RajanBabu & Reddy (1986). One crystal was subjected to six flashes to liberate phosphate and data collection initiated after a 24 h lag period during which it was anticipated that catalysis would take place. The second crystal was not flashed and data collection was started 48 h after the start of the soak to test the stability of the DNPP in the reaction mixture. Three-dimensional data to 2.3 Å resolution were recorded on a Siemens–Nicolet Xentronics area detector with graphite monochromated CuKα radiation from a Rigaku rotating anode X-ray generator (60 kV, 60 mA). Each data-set took about 24 h to record. Data were processed with the XENGEN program suite (Howard *et al.* 1987). The data were about 80% complete to 2.3 Å with merging R values between symmetry related reflections of 0.075 (83 582 measurements; 35 296 unique reflections) and 0.080 (81 689 measurements; 34 609 unique reflections) for the flashed and non-flashed crystals respectively. After scaling to the native GP*b* data-set, the fractional changes in structure factor amplitudes were 0.134 and 0.117 for the flashed and non-flashed crystals respectively.

The resulting difference map from the crystal that had not been flashed showed binding of heptenitol at the catalytic site and no evidence of catalysis (figure 2*a*).

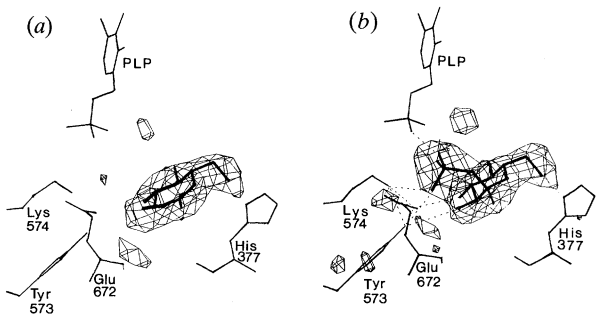

Figure 2. Difference electron density maps with data measured with monochromatic radiation on a Siemens–Nicolet Xentronics area detector. (*a*) Heptenitol bound in the presence of DNPP with no flash. (*b*) Heptulose-2-P formed 48 h after photolysis of DNPP to release phosphate.

DNPP was stable in the crystal under these conditions and the molecule was observed to bind at the allosteric effector site, where the binding was mostly through the DNPP phosphate interaction with the two arginine residues, Arg 309 and Arg 310, and at the nucleoside inhibitor site where the binding was directed through the interaction of the aromatic component of DNPP sandwiched between two aromatic residues Phe 285 and Tyr 613. The difference map obtained from the crystal that had received six flashes showed heptulose-2-P bound at the catalytic site (figure 2*b*) and unreleased DNPP bound at the allosteric effector site and a mixture of the released cage dinitrophenol and unreleased DNPP bound at the inhibitor site. This encouraging result showed that sufficient phosphate had been released to promote catalysis over the 48 h period (24 h rest and 24 h data collection). Subsequent experiments showed that catalysis had occurred within 24 h of flashing (i.e. data collection was begun immediately after six flashes) but that a single flash provided insufficient phosphate for the reaction to go to completion in 48 h.

3. Laue diffraction experiments

A crystal (dimensions approximately 1.6 mm × 0.4 mm × 0.4 mm) of native T state GP*b* was soaked in a solution containing 50 mM heptenitol, 45 mM dinitrophenylphosphate (DNPP), 10 mM BES, 10 mM magnesium acetate, pH 6.7 for 0.5 h at room temperature (about 20 °C) in a quartz capillary tube. The crystal was mounted on the oscillation camera at station 9.7, at the Synchrotron Radiation Source, Daresbury with the c^* axis inclined 5.2° to the X-ray beam. The orientation of the a^* axis to the X-ray beam was random. The crystal to film distance was 130 mm; collimator size 200 μm; circulating current of the synchrotron was about 200 mA throughout the experiments. For each time-resolved experiment, three Laue photographs were recorded at $\phi = 0°$, 11.5° and 23° with exposures of 800 ms per photograph. The X-ray film was CEA reflex and a six film pack (labelled films A to F) was used with no interleaving foil. After each time shot of three photos the crystal was translated to expose a fresh portion of the crystal. The first Laue photos were recorded before flashing (dark). The crystal was then removed from the hutch and flashed five times with an xenon flash lamp as described above. The total time to flash the crystal was about 30 s because after each 1 ms flash the lamp required a recovery period of 5 s. The crystal was returned to the hutch and three Laue photos recorded at 3 min (2 min 29 s, 3 min 8 s, 3 min 47 s); 15 min (14 min 39 s, 15 min 16 s, 15 min

PHILOSOPHICAL TRANSACTIONS OF THE ROYAL SOCIETY A MATHEMATICAL, PHYSICAL & ENGINEERING SCIENCES

54 s); and 1 h (58 min 52 s, 59 min 30 s, 1 h 8 s) where zero time was taken as the time for the first flash. The space in the hutch on station 9.7 is restricted and it was not possible to flash the crystal *in situ* on the camera. A rate limiting step in the experiment was the time taken to replace the crystal after flashing (about 2 min). A further rate limiting step was the time taken to rotate the crystal 11.5° and to advance the carousel between photos (about 35 s).

Films were scanned with a 50 μm spot and raster on an Optronics P-1000 microdensitometer and processed using the CCP4 programme package (Machin *et al.* 1985; Campbell *et al.* 1987; Helliwell *et al.* 1989). The photos and the crystal orientation parameters showed that a significant movement of the crystal (a change in Φ_Z of about 8°) had occurred after flashing. This meant that the data could not be normalized using the DIFFLAUE procedure in which data are scaled to a native reference Laue set (Hajdu *et al.* 1987*b*). In a trial run only the A films for the dark and 1 h experiments were processed. Spot predictions to 2.5 Å resolution gave root mean square (RMS) deviations of between 0.057 and 0.071 mm for the dark experiment and 0.055 and 0.087 for the 1 h experiment. Integration of intensities was performed with INTLAUE. Intensities of reflections whose separations were between 0.2 and 0.1 mm were deconvoluted (Shrive *et al.* 1990) and those whose separations were less than 0.1 mm where rejected. The data were normalized to a single wavelength with LAUENORM in the wavelength ranges 0.5–0.9 Å and 0.95–2 Å. The program derives appropriate scale factors from a comparison of the intensities of symmetry related reflections that have been recorded at different wavelengths. The lower cut off of 0.5 Å was chosen to optimize the merging R agreement. Reflections were rejected if intensities were less than 3σ. For the dark experiment some 11833 reflections (35% complete to 2.5 Å) with merging R of 0.11 and for the 1 h experiment 9392 reflections (27% complete to 2.5 Å) with a rather poorer merging R of 0.17 were obtained. The data were scaled to the native phosphorylase data set and difference maps calculated using coefficients $F_L - F_N$, where F_L and F_N are the structure factor amplitudes for the liganded complex obtained from normalized scaled Laue data and the native phosphorylase data respectively and phases calculated from the refined coordinates of the native structure with Sim weights.

The difference maps were disappointing. The dark map indicated that heptenitol was bound at the catalytic site but the density was fragmented with no density for C5–O6 or for O5 and the signal-to-noise was poor. The map for the 1 h experiment was worse which was probably a result of the poorer quality data and fewer reflections. At this stage trial studies with ideal data were carried out to assess the consequences of partial data sets on Laue difference maps.

4. Effects of partial data on difference maps

Calculations show that 25213, 21713 and 16252 unique reflections are potentially recordable at the three ϕ angles, respectively, under the conditions described in §3. After merging, these give a unique set of 29304 unique reflections that comprise 87% of the data to 2.5 Å resolution (figure 3). Thus in principle the Laue geometry at this crystal setting allows nearly a full set of data to be recorded in three shots. (Indeed the first two photos at 0 and 11.5° yielded 29099 unique reflections). In practice, Laue data-sets are incomplete for a number of reasons. A substantial proportion of reflections are rejected in the data processing because intensities are judged unreliable if $I < 3\sigma$, because reflections are too close in space to deconvolute if their

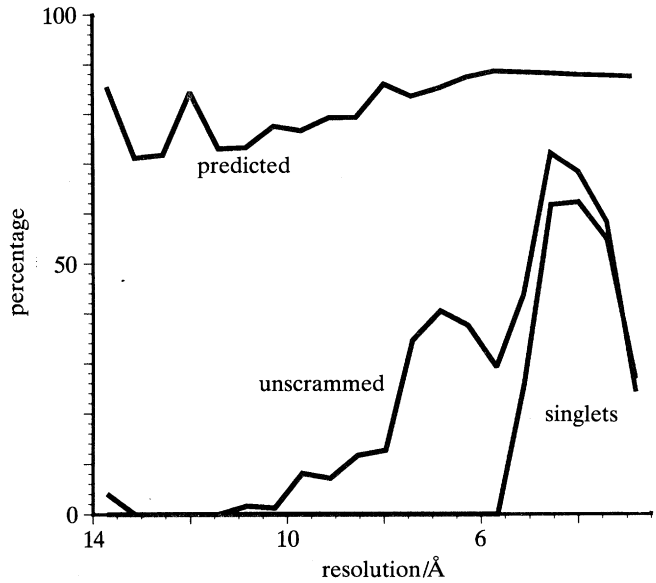

Figure 3. Diagram of percentage completeness of Laue data against resolution. 'Predicted' corresponds to all reflections that are recorded on the photographs for the 3ϕ settings (see text). 'Singlets' corresponds to the 11 K reflections obtained without unscrambling harmonic overlaps. 'Unscrammed' corresponds to the 13 K reflections obtained when harmonic overlaps are unscrambled and included in the data.

spot separation is less than 0.1 mm, because harmonic reflections generated by different wavelengths that superimpose on the photograph are not unscrambled and because of wavelength cut-offs introduced in the data processing to optimize precise measurements. For the dark experiment, these limitations reduced the nominal 29304 reflections potentially recordable to a measured set of 11833 reflections (35% of the complete data set) (figure 3) and these lack all data below 5 Å resolution. Many of the low resolution terms that are recorded have not been measured because of the 0.5 Å lower wavelength limit imposed in LAUENORM where reflections recorded at short wavelength appeared to give poor agreement and because wavelength multiplets have not been unscrambled. Cruickshank *et al.* (1987) showed that the proportion of wavelength multiplets represent a small fraction of the complete data set (about 17% when all rays can be recorded on the film). However, the low resolution terms are more significantly affected. For an infinite bandwidth of $\lambda_{\min} = 0$ and $\lambda_{\max} = \infty$, Cruickshank *et al.* show that all spots which are recorded at resolutions lower than $2\,d_{\min}$ (where $d_{\min}$ is the resolution limit for diffraction by the crystal) are multiplets. Some assessment of the effects of partial data-sets for protein electron density maps has been given by Farber *et al.* (1988) and Hajdu *et al.* (1991).

A series of difference maps based on calculated structure factors have been examined to assess the effects of partial data on Laue difference maps with phosphorylase. Structure factors were calculated for data between 200 and 2 Å for native phosphorylase and phosphorylase complexed with the glucose analogue inhibitor, 1-deoxy, 1-amido-α-D-glucose. The structures used were those previously obtained from refinement and included individual temperature factors and water molecules. The phosphorylase–ligand structure had recently been refined (K. Woods and K. Veluraja, unpublished work) and coordinates were readily available for use

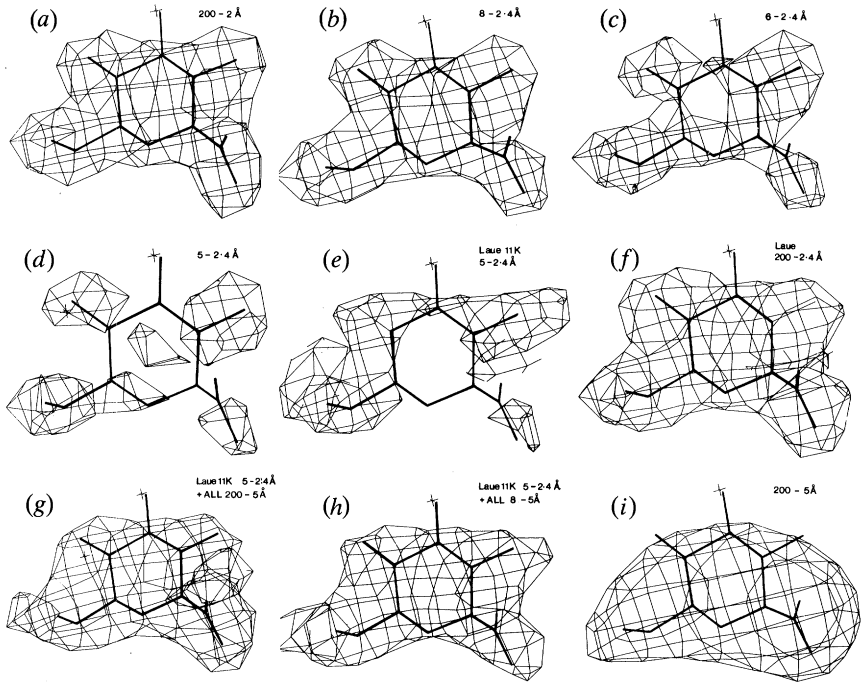

Figure 4. A series of difference electron density maps for 1-deoxy,1-amido-α-D-glucose bound at the catalytic site of phosphorylase computed with calculated structure factors for both protein and protein plus ligand and with native protein phases Sim weighted (*a*) All data between 200 and 2 Å resolution. (*b*) All data between 8 and 2.4 Å resolution. (*c*) All data between 6 and 2.4 Å resolution. (*d*) All data between 5 and 2.4 Å. (*e*) The 11 K reflections for the Laue data as selected in the Dark experiment. (*f*) The predicted Laue data if all reflections recorded on the films were measurable. (*g*) The 11 K Laue data-set with the addition of all terms between 200 and 5 Å resolution. (*h*) The 11 K Laue data-set with the addition of all data between 8 and 5 Å resolution. (*i*) All data between 200 and 5 Å resolution.

in the trials. The resulting difference map based on the calculated structure factors and phases calculated for reflections observed in the native data set weighted with Sim weights is shown in figure 4*a*. With the complete data the atoms of the modified glucose molecule are distinguished except for the O3 atom which displaces a water molecule from the native structure and hence does not have density in the difference map. Truncation of the data set to 8–2.4 Å had little effect on the general appearance of the difference map as seen in the projection (figure 4*b*) but examination in three dimensions showed some loss of detail from the loss of high resolution terms. Further truncation of the low resolution terms resulted in deterioration of the difference map. The map based on 6–2.4 Å data was poor and the map based on a 5–2.4 Å data-set was almost uninterpretable (figure 4*c*, *d*). The limit for the low resolution data appeared to be about 5.6 Å. A map based on those data present in the Laue data-set (dark) that contains 11 833 terms (Laue 11 K map) was poor (figure 4*e*). A difference map calculated from all the data (29 304) recordable from three Laue photos was good (figure 4*f*). The 11K Laue data-set not only lacks the low resolution terms but also contains partial data for the remainder of the data-set (figure 3). Addition of the low resolution terms to this data-set had a dramatic effect. Addition of the 200–5 Å complete data to the 11 K map resulted in an interpretable map (figure 4*g*).

Significant improvements were also obtained if the 200–8 Å or just the 8–5 Å data were added (figure 4*h*). The appearance of the 5 Å difference map is shown in figure 4*i* and it is clear that the higher resolution terms in the Laue data-set maps are contributing to the detail that defines the structure. Addition of low-resolution terms with structure factors equal to the average value for that range did not result in any improvement (data not shown) indicating that the improvements described above are dependent on correct structure factors and not general low-resolution terms.

The consequences of partial data can be examined through the effects of the appropriate point spread function. If the structure factor $F(\boldsymbol{S})$ and electron density $\rho(\boldsymbol{r})$ equations are represented as continuous integrations

$$F(\boldsymbol{S}) = \int \rho(\boldsymbol{r}) \exp(2\pi \mathrm{i} \boldsymbol{r}\cdot\boldsymbol{S})\,\mathrm{d}V, \quad \rho(\boldsymbol{r}) = \int F(\boldsymbol{S}) \exp(-2\pi \mathrm{i} \boldsymbol{r}\cdot\boldsymbol{S})\,\mathrm{d}V^*,$$

where $\boldsymbol{r}$ and $\boldsymbol{S}$ are real and reciprocal space vectors, $\mathrm{d}V$ and $\mathrm{d}V^*$ are the volume elements in real space and reciprocal space and the integrations are taken over the whole of the unit cell for $F(\boldsymbol{S})$ and the whole of reciprocal space for $\rho(\boldsymbol{r})$. The resulting electron density obtained with limited data is given by

$$\rho'(\boldsymbol{r}) = \int t(\boldsymbol{S}) F(\boldsymbol{S}) \exp(-2\pi \mathrm{i} \boldsymbol{r}\cdot\boldsymbol{S})\,\mathrm{d}V^*,$$

where $t(\boldsymbol{S}) = 1$ when a reflection is present and $t(\boldsymbol{S}) = 0$ otherwise. For example if the partial data lack terms below resolution S_1 then $t(\boldsymbol{S}) = 1$ if $S > S_1$ and $t(\boldsymbol{S}) = 0$ if $S < S_1$. By substituting into the structure factor equation (see, for example, Lipson & Cochran 1968, p. 323) it can be shown that $\rho'(\boldsymbol{r})$ is given by the convolution

$$\rho'(\boldsymbol{r}) = \int \rho(\boldsymbol{r}-\boldsymbol{R})\, T(\boldsymbol{R})\,\mathrm{d}V,$$

where the point spread function $T(\boldsymbol{R})$ is the Fourier transform of $t(\boldsymbol{S})$, i.e.

$$T(\boldsymbol{R}) = \int t(\boldsymbol{S}) \exp(-2\pi \mathrm{i} \boldsymbol{R}\cdot\boldsymbol{S})\,\mathrm{d}V^*.$$

Thus in the modified electron density distribution $\rho'(\boldsymbol{r})$ the electrons in every volume element $\mathrm{d}\boldsymbol{R}$ at a distance $\boldsymbol{R}$ from $\boldsymbol{r}$ are modified by multiplication by $T(\boldsymbol{R})$ and contribute to $\rho'(\boldsymbol{r})$ by $\rho(\boldsymbol{r}-\boldsymbol{R})\ T(\boldsymbol{R})\,\mathrm{d}\boldsymbol{R}$. In the early days of crystal structure determination from electron density maps the effects of series termination errors arising from lack of high resolution terms were recognized and methods developed for their correction (see, for example, James 1948; Cruickshank 1949). The effect of loss of low resolution terms has been shown in optical transforms to give rise to a series of diffraction rings around the object (Harburn *et al.* 1975, Plates 31 and 32). For objects with a simple boundary between transparent and opaque regions the effect is to enhance the contrast at the boundary as in dark field optical microscopy. For more complex objects where the separation of detail is comparable to the dimensions of the diffraction rings, the contrast reversal effects make the image almost uninterpretable. Similar effects of the contrast transfer function have been recognised in phase contrast electron microscopy.

The analytical form of the function $T(\boldsymbol{R})$ for the loss of high resolution terms ($S > S_{\max}$) with the assumption of an infinitely large unit cell was shown by James

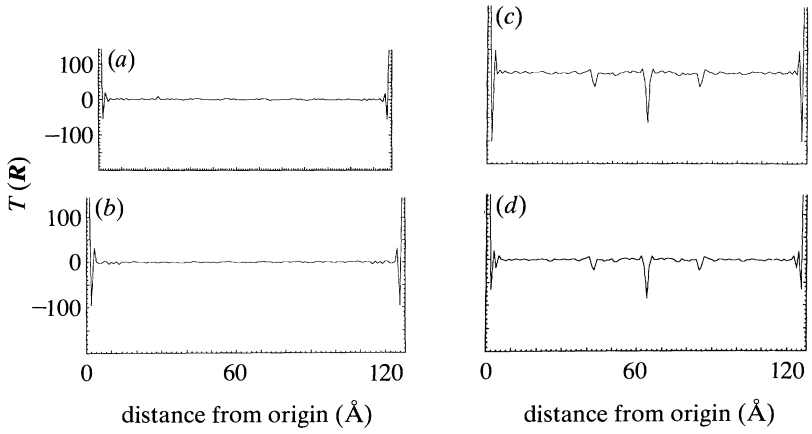

Figure 5. A section of the point spread function $T(\boldsymbol{R})$ against distance from the origin in the direction of the crystallographic a axis. The height at the origin of each function is 1000. (*a*) For the data-set 200 to 2.5 Å resolution. (*b*) For the data-set 5 to 2.4 Å resolution as in figure 4*d*. (*c*) For the Laue data set of 11 K reflections from the dark experiments as in figure 4*e*. (*d*) The Laue data set of 11 K reflections plus the full data set to 5 Å resolution as in figure 4*g*.

(1948) to be $T(\boldsymbol{R}) = \frac{4}{3}\pi(S_{\max}^3\, \Phi(2\pi R S_{\max}))$, where $\Phi(x) = 3(\sin x - x\cos x)/x^3$. It can be shown that the function where data are limited between the resolution limits of $S_{\min}$ and $S_{\max}$ is given by:

$$T(\boldsymbol{R}) = \tfrac{4}{3}\pi(S_{\max}^3\, \Phi(2\pi R S_{\max})) - \tfrac{4}{3}\pi(S_{\min}^3\, \Phi(2\pi R S_{\min})).$$

This expression has been calculated for $S_{\max} = 0.4$ Å^{-1} and $S_{\min} = 0$ and for $S_{\max} = 0.4$ Å^{-1} and $S_{\min} = 0.2$ Å^{-1}. As illustrated in James (1948), the curves show a central maximum at $R = 0$ surrounded by diffraction ripples. For the resolution limits ∞ to 2.5 Å the first minimum occurs at $R = 2.3$ Å with a depth 8.7 % of the origin peak. For the resolution limits of 5–2.5 Å the first minimum occurs at the same position but is broader and has a depth 15 % of the origin peak.

To incorporate the effects of unit cell and space group and the distribution of terms in an experimental data set, the function $T(\boldsymbol{R})$ has been evaluated numerically using the Fourier transform routine. The results shown in figure 5. The curves show a section of the point spread function along the a axis of the unit cell. With the selection of data used in the maps the function is not spherically symmetric but the a axis section is fairly typical. In the calculation of the electron density maps the Fourier summation is normalised to 1000 for the highest peak. Likewise the point spread functions have been normalized to a value of 1000 at the origin. For the full data-set to 2.5 Å (figure 5*a*) there are diffraction rings around the origin with a first minimum at about 2 Å with a depth of −55. (The function was calculated with a relatively coarse grid of 1 Å and values for position and depth are approximate.) The function for the restricted data set of 5–2.4 Å (figure 5*b*) shows a broader and more pronounced minimum of −100. For the limited Laue data set of 11 K reflections (figure 5*c*) the minimum is −150 and there are long range perturbations at $\frac{1}{3}$ and $\frac{1}{2}$ of the unit cell that arise from the systematic absence of harmonic reflections that arise from wavelength overlaps and were not unscrambled in the data processing. It is anticipated that these features will distort the Fourier synthesis as indeed is observed. Addition of the low resolution terms (200–5 Å) to the limited Laue set

(figure 5*d*) reduces the first minimum to −65 although the longer range fluctuations are not significantly altered. Inclusion of the harmonic overlaps from the Laue data set diminishes the troughs at $\frac{1}{2}$ and $\frac{1}{3}$. In these calculations the function represents the transform for a point atom at rest. A more realistic representation of the loss of low resolution terms from electron density maps could be obtained by using an atom spread function in which the amplitude of 1 for each term is replaced by $f \exp(-B\sin^2\theta/\lambda^2)$, where f is the atomic scattering factor and B is an appropriate temperature factor (Cruickshank 1949). The atom spread function will spread the atomic image by the convolution of the static atom density modified by the temperature factor gaussian with the finite series point spread function. When the low angle data are missing, the atom spread function will give greater relative weight to the missing terms because of their greater magnitude compared with the higher resolution terms.

Taken together with the observations from the calculated maps the results suggested that the low resolution terms contribute to the difference maps and that it is worth rescuing these terms from the Laue data. The effects are likely to be of greater importance for the identification of molecules in Fourier syntheses where the separation of non-bonded atoms is of the same order of magnitude as the diffraction rings (as in the glucopyranose ring) and will be of less importance in work that aims to identify single heavy atoms such as iron or calcium.

5. Effects of unscrambling wavelength overlap reflections

Examination of the Laue data-sets indicated that large proportion of reflections below 5 Å resolution had been rejected because they were multiplets arising from harmonic reflections generated at different wavelengths. The data were reprocessed with AFSCALE, a program that derives scale factors as a function of wavelength for the A to F films in a film pack. The Victoreen coefficients for the wavelength correction curves were used to unscramble the multiplet reflections with UNSCRAM in the wavelength range 0.2 to 2.1 Å. The program uses the different film–film ratios between intensity measurements on successive films at different wavelengths to calculate (unscramble) the individual single wavelength component reflections. The results are shown in table 1. The merging R values obtained from AFSCALE for the six film packs for each of the experiments ranged between 0.07 and 0.10 for the first two ϕ settings but was larger (between 0.11 and 0.15) for the third ϕ setting probably indicating some radiation damage. The data were normalized with LAUENORM (wavelength range 0.5–0.9; 0.95–2.1 Å). Comparison of merging R values with and without the additional terms showed no worsening of agreement among symmetry related reflections from unscrambling the multiplets. For the dark experiment the number of reflections was increased from 11833 to 13373 corresponding to 40% of the complete data-set (figure 3) with a significant increase in the low resolution terms. About 300 of the increase of 1540 reflections arose from reflections that had been too strong to measure on the A films and the remainder from unscrambling the multiplets. For the 3 min and 1 h experiments several trials were performed to try to produce the best data-set and some improvement was obtained by omission of the spatial overlap reflections. For the 15 min experiment the data from the third film pack were omitted.

The resulting difference electron density maps showed improvement. In the dark map the difference electron density clearly indicated heptenitol bound (figure 6). The

PHILOSOPHICAL TRANSACTIONS OF THE ROYAL SOCIETY A MATHEMATICAL, PHYSICAL & ENGINEERING SCIENCES

PHILOSOPHICAL TRANSACTIONS OF THE ROYAL SOCIETY A MATHEMATICAL, PHYSICAL & ENGINEERING SCIENCES

Table 1. *Data processing statistics for the time resolved Laue experiment including unscrambling of wavelength overlap reflections*

	dark			3 min[a]			15 min			1 h[a]		
AFSCALE												
film	1A–F	2A–F	3A–F	4A–F	5A–F	6A–F	7A–F	8A–F	9A–F	10A–F	11A–F	12A–F
no. output	30516	29903	30921	22298	22461	22333	29706	30221	29757	23101	23062	22532
merging R[b]	0.089	0.098	0.111	0.073	0.078	0.086	0.081	0.084	0.158	0.107	0.099	0.147
UNISCRAM												
no. unscrambled[c]	1930	1951	1957	1937	1986	1573	1950	1954	1207	1869	1720	1092
LAUENORM	packs 1, 2, 3			packs 4, 5, 6			packs 7, 8			packs 10, 11, 12		
no. accepted	32819			27519			22741			23467		
no. rejected[d]	64359			45069			41090			49909		
no. output	13373			11213			10 937			9735		
merging R	0.098			0.141			0.106			0.105		
$\Delta F/F$	0.148			0.191			0.172			0.173		
% complete	40			38			32			29		

[a] Excluding all spatial overlapped spots (separation < 0.2 mm).

[b] Merging R for AFSCALE is $R = \Sigma_h\ (\Sigma_i |I - I_i|/n)/\Sigma_h I$ where the summation is over all reflections and all the films A to F for which a reflection is present. I is the mean value and I_i the scaled intensity of the ith film respectively and n is the number of films with reflection present. The expression includes reflections even if only one measurement is present and hence is an optimistic estimate of agreement.

[c] In film A1 the 1930 multiplets comprised 1673 doublets, 247 triplets and 10 others.

[d] Reflections rejected if $I < 3\sigma$, or if $I < 0$, or if wavelength at which reflections is recorded is outside the wavelength limits.

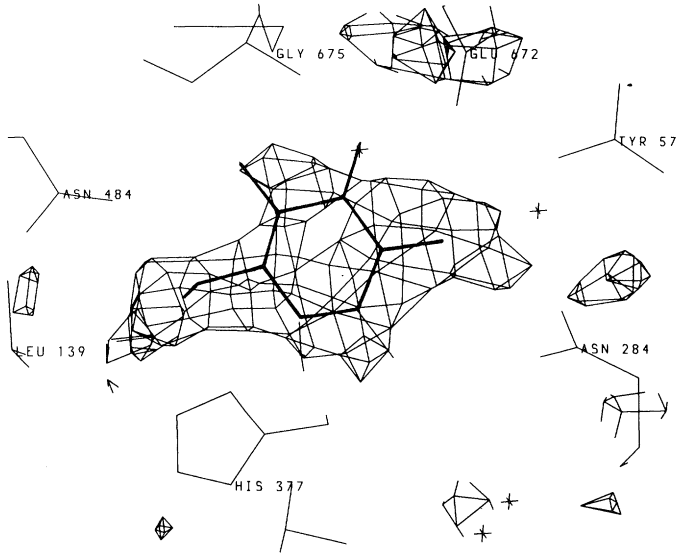

Figure 6. Difference electron density map for the dark experiment with Laue data after harmonic overlaps have been unscrambled (see table 1). Heptenitol and some of the adjacent residues are shown at the catalytic site. The O3 hydroxyl displaces a water molecule and hence no electron density is observed in the difference map.

15 min map was also of sufficient quality to identify heptenitol with confidence. The maps for the 3 min and 1 h experiments were poor although there was indication of bound heptenitol.

Comparison of the dark and 15 min maps showed some density that could represent the phosphate in the attacking position between the heptenitol and the cofactor 5′-phosphate in the 15 min map but the noise in the map did not allow an unambiguous assignment. Heptulose-2-P occupies a slightly different position from heptenitol (a shift in the ring by about 0.3 Å). In all three maps after phosphate had been released (3 min, 15 min and 1 h) the density corresponded to the position of heptenitol and not heptulose-2-P. It was concluded that little or no catalysis had occurred in the crystal under these conditions.

6. Conclusions

The results presented in this manuscript show some progress towards good quality Laue difference maps with glycogen phosphorylase. Incorporation of low-resolution terms and unscrambling of the wavelength multiplets have been shown to be important from theory, numerical calculations and experiment for interpretable difference maps of compounds containing a glucopyranose ring. Nevertheless, we are aware that good difference maps have been obtained for a number of other proteins without unscrambling wavelength overlaps (such as work with H-ras p21, trypsin, γ-chymotrypsin, cytochrome C peroxidase and carbonic anhydrase, as reported elsewhere in this volume). These proteins are smaller than glycogen phosphorylase (molecular mass 100000) and most of the ligands bound to the other proteins exhibit much higher affinity than the ligands bound to phosphorylase. For phosphorylase the problem of difference maps from Laue data may be exacerbated by the large number of weak reflections $I < 3\sigma$ that have been omitted from the data-set. These

comprise about 60% of the measurements. Future efforts will be directed towards enhancement of data quality from modified software that allows improvements in the deconvolution of spatial overlaps and estimations of background measurements (S. Wakatsuki, unpublished results).

Experiments with caged phosphate and X-ray data collected using monochromatic radiation have shown that sufficient phosphate can be released to promote catalysis within the 24 h period of data collection. The Laue experiments have shown that little or no catalysis has occurred during the 1 h period of that experiment and there is no clear indication of phosphate binding in the attacking position. Although the Laue experiments were performed under slightly different conditions to the measurements on release of phosphate using the diode array spectrophotometer, a rough calculation, assuming release is proportional to concentration, suggests that between 7 mM and 15 mM might have been released from the caged phosphate in the Laue experiment. This appears insufficient to saturate the phosphate recognition site and to promote phosphorolysis. (The concentration of the enzyme in the crystal is about 7 mM.) It is of interest that the 3 min Laue photos showed no transient disorder after release of phosphate in contrast to the transient disorder that is observed when high concentrations of phosphate are diffused into the crystal. Glycogen phosphorylase presents an especially difficult problem because of the low affinity for phosphate in the T state. It may be necessary to return to the diffusion method to achieve sufficiently high concentrations in the crystal. Alternatively, the R state has a high affinity for phosphate as observed in the crystals of R state phosphorylase where a dianion is already bound at the catalytic site (Barford & Johnson 1989). However the R state crystals have a larger unit cell (one axis 190 Å), have a less favourable spacegroup ($P2_1$) for collection of Laue data and tend to exhibit some disorder. Hence it will be an advantage to have established optimum protocols for Laue data before tackling this more challenging crystal form.

Note added in proof (*4 June 1992*). All four Laue data-sets (dark, 3 min, 15 min and 1 h) have been reprocessed with a new intensity integration protocol that permits improved measurements of spatially overlapped spots, background and standard deviations (S. Wakatsuki, unpublished results). With inclusion of unscrambled wavelength overlap reflections, the improved intensity measurements result in difference maps in which the bound ligand is clearly and unambiguously recognized. The new maps confirm that catalysis had not taken place on the timescale of the experiment.

We gratefully acknowledge Dr D. R. Trentham and G. P. Reid for gifts of DNPP; Dr G. W. R. Fleet and Dr I. Bruce for gift of heptenitol; Dr E. F. Garman for help with the Siemens area detector; Dr J. Hajdu and D. W. J. Cruickshank for stimulating discussions and I. Clifton for advice. This work has been supported by the Medical Research Council and the Science and Engineering Research Council. L.N.J. is a member of the Oxford Centre for Molecular Sciences.

References

Acharya, K. R., Stuart, D. I., Varvill, K. M. & Johnson, L. N. 1991 *Glycogen phosphorylase: description of the protein structure*. London and Singapore: World Scientific.

Barford, D. & Johnson, L. N. 1989 The allosteric transition of glycogen phosphorylase. *Nature, Lond.* **340**, 609–614.

Barford, D. & Johnson, L. N. 1992 The molecular mechanism for the association of glycogen phosphorylase dimers promoted by protein phosphorylation. *Protein Sci.* **1**, 472–492.

Barford, D., Hu, S.-H. & Johnson, L. N. 1991 Structural mechanism for glycogen phosphorylase control by phosphorylation and AMP. *J. molec. Biol.* **218**, 233–260.

Campbell, J. W., Clifton, I. C., Elder, M., Machin, P. A., Zurek, S., Helliwell, J. R., Habash, J., Hajdu, J. & Harding, M. M. 1987 In *Biophysics and synchrotron radiation* (ed. A. Bianconi & A. Congiucastellano), pp. 53–60. New York: Springer.

Cruickshank, D. W. J. 1949 Accuracy of electron density maps in X-ray analysis with special reference to dibenzyl. *Acta crystallogr.* **2**, 65–82.

Cruickshank, D. W. J., Helliwell, J. R. & Moffat, K. 1987 Multiplicity distribution of reflections in Laue diffraction. *Acta crystallogr.* A**43**, 656–674.

Duke, E. M. H., Hadfield, A., Martin, J. L., Clifton, I. J., Hadju, J., Johnson, L. N., Reid, G. P., Trentham, D. R., Bruce, I. & Fleet, G. W. R. 1991 Towards time resolved diffraction studies with glycogen phosphorylase. In *Protein Conformation Ciba Foundation Symposium*, vol. **161**, pp. 75–90. Chichester: Wiley.

Engers, H. D., Shechosky, S. & Madsen, N. B. 1970 Kinetic mechanism of phosphorylase *a*. *Can. J. Biochem.* **48**, 746–754.

Farber, G. K., Machin, P. A., Almo, S. C., Petsko, G. A. & Hajdu, J. 1988 X-ray Laue diffraction from crystals of xylose isomerase. *Proc. natn. Acad. Sci. U.S.A.* **85**, 112–115.

Hajdu, J., Acharya, K. R., Stuart, D. I., McLaughlin, P. J., Barford, D., Oikonomakos, N. G., Klein, H. & Johnson, L. N. 1987*a* Catalysis in the crystal: synchrotron radiation studies with glycogen phosphorylase *b*. *EMBO J.* **6**, 539–546.

Hajdu, J., Almo, S. C., Farber, G. K., Prater, J. K., Petsko, G. A., Wakatsuki, S., Clifton, I. C. & Fulop, V. 1991 On the limitations of the Laue method when applied to crystals of macromolecules. In *Crystallographic computing 5: from chemistry to biology* (ed. D. Moras, A. D. Podjarny & J. C. Thierry), pp. 29–49. Oxford University Press.

Hajdu, U., Machin, P. A., Campbell, J. W., Greenough, T. J., Clifton, I. C., Zurek, S., Gover, S., Johnson, L. N. & Elder, M. 1987*b* Millisecond X-ray diffraction and the first electron density map from Laue photographs of a protein crystal. *Nature, Lond.* **329**, 115–116.

Harburn, G., Taylor, C. A. & Welberry, X. 1975 *Atlas of optical transforms*. London: G. Bell & Sons.

Hehre, E. J., Brewer, C. F., Uchiyama, T., Schlesselman, P. & Lehman, J. 1980 Scope and mechanism of carbohydrase action: stereospecific hydration of 2,6-anhydro-1-deoxy-D-gluco-hept-1-enitol catalysed by a- and β-glucosidases and an inverting exo-a-glucanase. *Biochem.* **19**, 3557–3564.

Helliwell, J. R., Habash, J., Cruickshank, D. W. J., Harding, M. M., Greenhough, T. J., Campbell, J. W., Clifton, I. C., Elder, M., Machin, P. A., Papiz, M. Z. & Zurek, S. 1989 The recording and analysis of synchrotron X-radiation Laue diffraction photographs. *J. appl. Crystallogr.* **22**, 483–497.

Helmreich, E. J. M. & Cori, C. 1964 The role of adenylic acid in the activity of glycogen phosphorylase. *Proc. natn. Acad. Sci. U.S.A.* **51**, 131–138.

Howard, A. J., Gilliland, G. L., Finzel, B. C., Poulos, T. L., Ohlendorf, D. H. & Salemme, F. R. 1987 *J. appl. Crystallogr.* **20**, 383–387.

James, R. W. 1948 False detail in three-dimensional Fourier representations of crystal structures. *Acta crystallogr.* **1**, 132–134.

Johnson, L. N., Hajdu, J., Acharya, K. R., Stuart, D. I., McLaughlin, P. J., Oikonomakos, N. G. & Barford, D. 1989 Glycogen phosphorylase. In *Allosteric enzymes* (ed. G. Herve), pp. 81–127. Boca Raton, Florida: CRC Press.

Johnson, L. N. & Hajdu, J. 1989 Synchrotron studies on enzyme catalysis in crystals. In *Biophysics and synchrotron radiation* (ed. S. Hasnain), pp. 142–155. Chichester: Ellis Horwood.

Johnson, L. N., Acharya, K. R., Jordan, M. D. & McLaughlin, P. J. 1990 Refined crystal structure of the phosphorylase heptulose-2-phosphate oligosaccharide-AMP complex. *J. molec. Biol.* **211**, 645–661.

Kaplan, J. H., Forbush, B. & Hoffman, J. F. 1978 Rapid photolytic release of adenosine 5′-triphosphate from a protected analogue: utilisation by the Na:K pump of human red blood cell ghosts. *Biochem.* **17**, 1929–1935.

PHILOSOPHICAL TRANSACTIONS OF THE ROYAL SOCIETY A MATHEMATICAL, PHYSICAL & ENGINEERING SCIENCES

Kasvinsky, P. J. & Madsen, N. B. 1976 Activity of glycogen phosphorylase in the crystalline state. *J. biol. Chem.* **251**, 6852–6859.

Klein, H., Im, M.-J. & Palm, D. 1986 The role of pyridoxal 5′-phosphate and orthophosphate in general acid-base catalysis by α-glucan phosphorylases. *Euro. J. Biochem.* **157**, 107–114.

Lipson, H. & Cochran, W. 1968 *The determination of crystal structures*. London: G. Bell & Sons.

Machin, P. A. & Harding, M. M. (eds) 1985 *Information quarterly for protein crystallography*, vol. 15. Warrington: Daresbury Laboratory.

Madsen, N. B. & Withers, S. G. 1986 Glycogen phosphorylase. In *Coenzymes and cofactors*, vol. I, *vitamin B6 pyridoxal phosphate* (ed. D. Dolphin, R. Poulson & O. Avramovic) pp. 355–389. New York: John Wiley.

McCray, J. A. & Trentham, D. R. 1989 Properties and uses of photoreactive caged compounds. *A. Rev. Biophys. Biochem.* **18**, 239–270.

Oikonomakos, N. G., Johnson, L. N., Acharya, K. R., Stuart, D. I., Barford, D., Hajdu, J., Varvill, K. M., Melpidou, A. E., Papgeorgiou, D. J., Graves, D. J. & Palm, D. 1987 The pyridoxal phosphate site in glycogen phosphorylase b. The structure in the native enzyme and in 3 derivatives. *Biochem.* **26**, 8381–8389.

Palm, D., Klein, H. W., Schinzel, R., Buehner, M. & Helmreich, E. J. M. 1990 The role of pyridoxal 5′-phosphate in glycogen phosphorylase catalysis. *Biochem.* **29**, 1099–1107.

Parke, D. V. 1981 The metabolism of m-dinitrobenzeme in the rabbit. *Biochem. J.* **78**, 262–271.

RajanBabu, T. V. & Reddy, G. S. 1986 1-methylene sugars as C-glycoside precursors. *J. org. Chem.* **51**, 5458–5461.

Rapp, G. & Guth, K. 1988 A low cost high intensity flash device for photolysis experiments. *Euro. J. Physiol.* **411**, 200–203.

Schinzel, R. & Palm, D. 1990 *Escherichia coli* maltodextrin phosphorylase: contribution of active site residues Glutamate-637 and Tyrosine-538 to the phosphorolytic cleavage of a-glucans. *Biochem.* **29**, 9956–9962.

Schinzel, R. & Drueckes, P. 1991 The phosphate recognition sites of *Escherichia coli* maltodextrin phosphorylase. *FEBS Lett.* **286**, 125–128.

Shrive, A. K., Clifton, I. C., Hajdu, J. & Greenhough, T. J. 1990 Laue integration and deconvolution of spatially overlapping reflections. *J. appl. Crystallogr.* **23**, 169–174.

PHILOSOPHICAL TRANSACTIONS OF THE ROYAL SOCIETY A MATHEMATICAL, PHYSICAL & ENGINEERING SCIENCES